Journal of The Electrochemical Society, **158** (5) A523-A529 (2011)
0013-4651/2011/158(5)/A523/7/$28.00 © The Electrochemical Society

Neutron Imaging of Lithium Concentration in LFP Pouch Cell Battery

Jason B. Siegel,[a,*,z] Xinfan Lin,[a] Anna G. Stefanopoulou,[a] Daniel S. Hussey,[b,] David L. Jacobson,[b] and David Gorsich[c]**

[a]*Department of Mechanical Engineering, University of Michigan, Ann Arbor, Michigan 48109, USA*
[b]*National Institute of Standards and Technology Physical Measurements Laboratory, Gaithersburg, Maryland 20899-8461, USA*
[c]*U.S. Army Tank Automotive Research, Development and Engineering Center (TARDEC), Warren, Michigan 48397-5000, USA*

This paper shows how neutron radiography can be used for *in situ* quantification of the lithium concentration across battery electrodes, a critical physical system state. The change in lithium concentration between the charged and discharged states of the battery causes a change in number of detected neutrons after passing through the battery. Electrode swelling is also observed during battery charging. The experimental setup and the observations from testing a pouch cell with LFP cathode and graphite anode are reported here. The bulk Li concentration across the electrode and folds of the pouch cell is quantified at various states of charge. To interpret the measurements, the optics of the neutron beam (geometric unsharpness) and detector resolution are considered in order to quantify the lithium concentration from the images due to the thinness of the electrode layers. The experimental methodology provides a basis for comprehensive *in situ* metrology of bulk lithium concentration.
 [DOI: 10.1149/1.3566341]

Manuscript submitted December 6, 2010; revised manuscript received February 9, 2011. Published March 23, 2011.

Battery management requires accurate prediction of the bulk and the spatiotemporal lithium (Li) concentrations. The bulk concentration is a good metric for the total available energy stored in the battery. The spatial distribution is important for predicting the available power. In order to capture the spatial distributions, the electrode material has been modeled, since the early 90s, as a distribution of spherical particles along the electrode,[1,2] as shown in Fig. 1. Many renditions of this model exist, but in most cases sphere surface concentration of Li represents the amount of readily available power because the surface lithium is easily removed,[3,4] whereas the ions near the center of the particle are limited by the rate of diffusion to reach the surface and correspond to the bulk energy storage.

Although there are many distributed multi-scale physics-based models of the mass transport phenomena occurring inside the battery, they could all benefit from *in-situ* measurement of the lithium concentrations for model validation. Prior efforts to utilize neutron imaging resulted in only qualitative results.[5,6] Other *in-situ* Li measurement techniques using imaging may require visual access and therefore can provide only surface concentration information for the anode (carbon) electrode.[7] Neutron diffraction is another *in-situ* measurement tool that has been recently used to investigate Li-ion batteries.[8]

This manuscript includes observations of the raw data and a model of the imaging process. In order to provide quantitative information about the changes in bulk lithium concentration it is necessary to account for the effects of the imaging system when interpreting the results. We discuss the physics of the image formation process using pinhole optics, the Lambert-Beer law, material densities, and the neutron cross sections. A Lithium Iron Phosphate (LFP) pouch cell battery with typical commercial electrode materials was imaged using the thermal neutron imaging beamline at the National Institute for Standards and Technology (NIST) Center for Neutron Research.[9] Experiments were conducted with a high resolution Micro-Channel Plate (MCP) detector.

The experiments were carefully designed to achieve high measurement confidence in this initial effort. In this paper we show the *in situ* bulk lithium concentration measurements along the electrode thickness and length, at various states of charge and discharge, by imaging steady-state conditions, i.e., when the battery is at rest.

After a brief explanation of the experimental setup and the apparatus, the raw and processed images are presented. The battery structure (physical dimensions) and a model of the image formation system are used to interpret the data, since the resolution of the imaging system is only slightly smaller than the physical dimensions of the battery layers. Consecutive images at various states of charge and discharge show the Li movement between anode and cathode (by the local change in lithium concentration between frames). A 2% volume expansion is observed in the data due to material swelling during charging.

Principles of Lithium Metrology via Neutron Imaging

Neutron imaging is a valuable tool for *in situ* measurements. The principle of neutron imaging is similar to x-ray radiography, where a detector is placed behind an illuminated object to measure the change in transmission through that object. Neutron interactions with the battery reduce the number of transmitted neutrons. The neutron cross-sections, of various materials used in the construction of Li-ion batteries, indicate the probability of neutron interaction and are shown in Fig. 2. The neutron cross-section represents the attenuation that is due to both scattering and absorption. The relative strength of each processes depends on the specific isotope, and has been tabulated.[10]

Lithium's large cross section enables the study of changes in lithium atom concentration by measuring the change in neutron transmission. Hydrogen, like Li, also has a large neutron cross section. The successful utilization of neutron imaging for Fuel Cell (FC) liquid water metrology has been demonstrated at imaging facilities by NIST (Ref. 9) and Paul Scherrer Institute.[11] The FC liquid water measurements have advanced our understanding of the water dynamics and have been used to validate mathematical models of the complex spatiotemporal FC behavior.[12,13] These results motivated our development of neutron imaging techniques for validating Li-ion battery models.

The setup used for battery imaging is shown in Fig. 3. A neutron sensitive detector is placed behind the battery to measure the change in transmission and a beam of neutrons is directed at the sample.

The transmitted neutron beam intensity (I) is described by the Lambert-Beer Law using the composite neutron interaction probability of each independent material scaled with the molar concentration of that material. Since the battery is composed of many materials, we can write the total linear attenuation as the sum of two components, one which is changing over time, the lithium concentration, $c_{Li}(t)$ mol cm^{-3}, and one which remains stationary

* Electrochemical Society Student Member.
** Electrochemical Society Active Member.
z E-mail: siegeljb@umich.edu

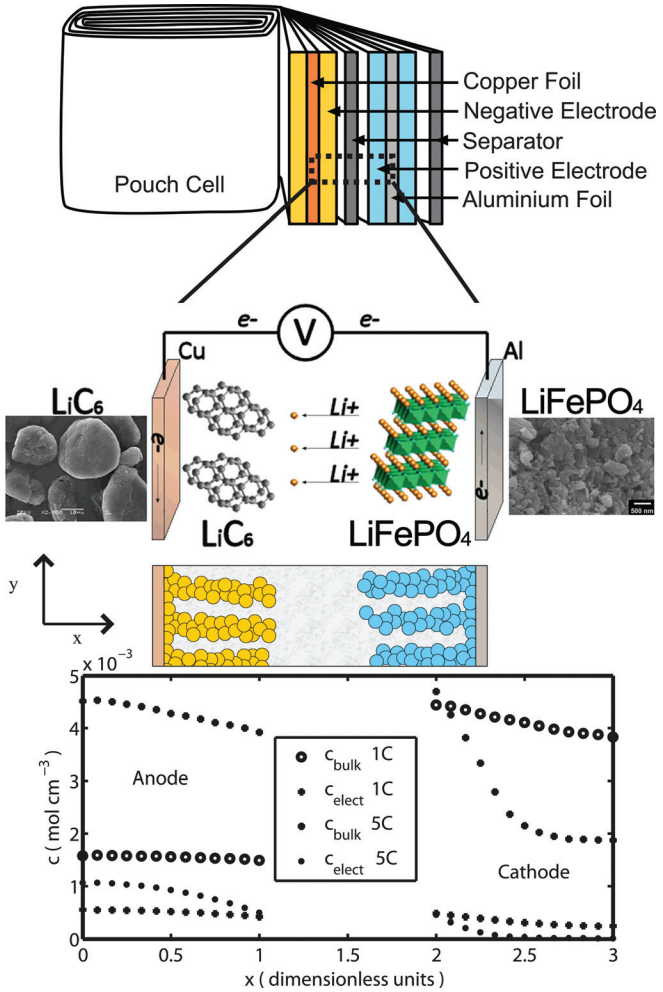

Figure 1. (Color online) The pouch cell construction used for neutron imaging is shown with an expanded view of the electrode structure. The lithium concentration distribution varies across the electrode in the solid and the electrolyte during battery discharging as a function of C-rate, using the battery model provided in Comsol.

$$I(t) = I_0 \exp\left(-\sigma_{Li} c_{Li}(t) N_A \delta - \sum_{i,i\neq Li} \sigma_i c_i N_A \delta\right) \quad [1]$$

where I_0 is the incident beam intensity, c_i is the molar concentration (mol cm^{-3}), N_A is Avogadro's Number, σ_i is the total neutron scattering cross section (cm^2) for element i, and δ is the thickness of the battery in the beam direction.

As Eq. 1 indicates, the neutron beam attenuation depends not only on the cross section σ, but also the number density of atoms N. In addition to having a large cross section, the concentration of lithium in the intercalation material is high and changes significantly between the charged and discharged states. The bottom panel in Fig. 1 shows an example of the solid bulk and electrolyte lithium concentrations across the electrode at two different C-rates. As can be seen, the largest change in molar concentration of lithium occurs within the intercalation materials. Measurement of the change in lithium ion concentration in the electrolyte is not feasible because the number density of lithium atoms in the solution is too low, and hence, the changes are imperceptible. However, due to the high neutron cross section of the hydrocarbon based solvents, neutron radiography has been used to see the absorption of the electrolyte into the battery electrode structure during initial cycling.[6]

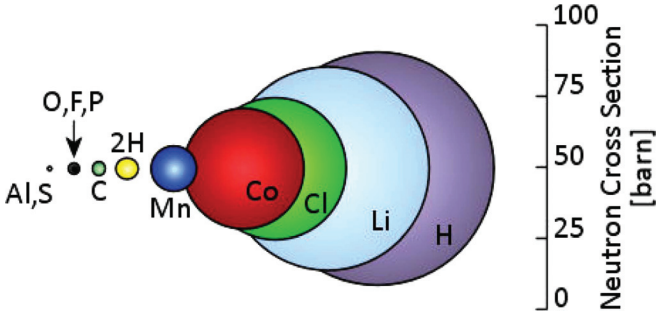

Figure 2. (Color online) Averaged total (scattering and absorbing) neutron cross-sections based on naturally occurring concentration of isotopes.[10]

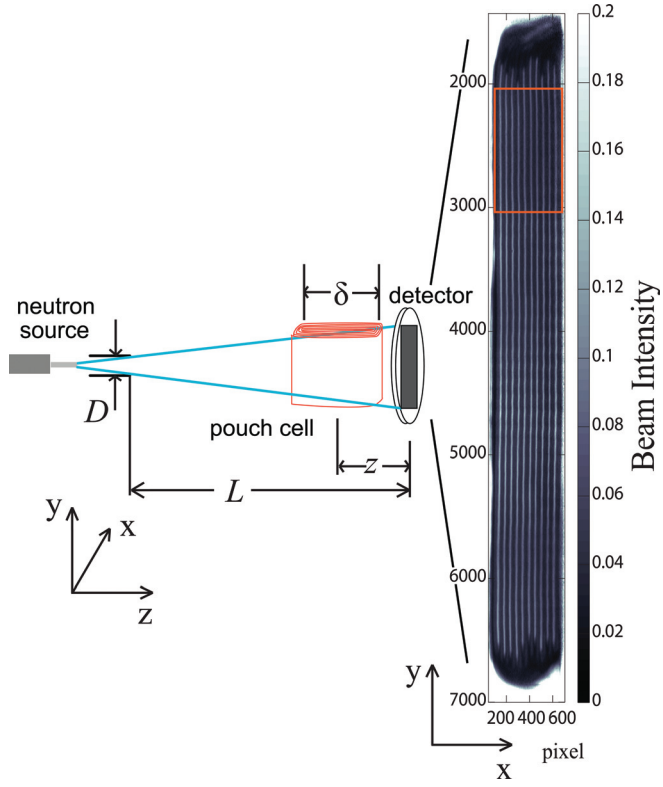

Figure 3. (Color online) (Left) Neutron imaging setup. The neutron beam is attenuated as it passes through the pouch cell to reach the detector, producing a 2D projection of the battery onto the x-y plane as shown in the right panel in Fig. 3. (Right) Neutron image of pouch cell. The battery width along the optical axis is $\delta = 2$ cm.

The optical axis bisects the anode and cathode electrodes, so that the change in local lithium atom density (integrated along the beam path) produces a local change in the number of neutrons transmitted through the battery forming a two-dimensional projection onto the *x-y* plane. The two dimensional (2D) position sensitive count of the number of neutrons that hit the detector is then recorded. The planar pouch-cell construction has a unique advantage over cylindrical designs for neutron imaging. When the optical axis is parallel to the plane of the separator the difference between anode and cathode layers are easily identified in the neutron image. Also in this orientation the Li-ion migration between the anode and cathode electrodes can be observed during charging or discharging. The electrode width δ, along the beam path, can also be tailored to optimize the beam transmission. Increasing δ can increase the effect of lithium concentration changes on neutron transmission, however, if it is too large not enough neutrons will reach the detector increasing the measurement uncertainty.

Measurement uncertainty arises primarily from the random nature of the neutron emission and interactions with the battery and detector. The number of neutrons counted in a given period of time

can be described by a Poisson distribution. In order to minimize the measurement uncertainty, we should increase the number of counted neutrons, which can be achieved by careful choice of materials, increasing the exposure time, and/or by spatial averaging.

Experimental

This section describes the testing protocol and the steady state conditions under which neutron images were acquired. Low current rates were applied to the battery in order to ensure a flat distribution of lithium concentration across the solid electrode.[14,15] The low current rate also enables increasing the effective exposure time which yielded lower noise and higher confidence in lithium concentration measurement.

Neutron Source.— The neutron imaging setup is similar to a pinhole camera. The geometry of the imaging setup, shown in Fig. 3, impacts the sharpness of the resulting image, which can limit the spatial resolution of the neutron imaging based Li metrology. The geometric unsharpness can be modeled by convolving a sharp image with a pillbox function of width $U_g = zD/L$, which is also equal to the full width at half maximum (FWHM). The FWHM describes the spatial separation at which two Gaussian distributed signals become indistinguishable. Care must be taken to ensure that the FWHM of the geometric unsharpness is much smaller than that of the detector, otherwise the overall system resolution will be less than that of the detector. The separation between the aperture and the detector, $L = 6$ m, is constrained and fixed at the NIST facility. The neutron beam divergence at the sample location and the neutron beam intensity both depend on the aperture size D. The ratio of these quantities, L/D, and the neutron flux define the capability of the imaging facility.[9,16] An $L/D = 3000$ is used for the experimental setup reported here. The distance z between the detector and the battery is also a critical parameter of the imaging system. For the experimental setup $z = 5.4$ cm, so the theoretical geometric unsharpness is $U_g = 18$ μm.

Increasing the *L/D* ratio, by decreasing the aperture diameter, decreases the geometric unsharpness, but the trade-off is lower neutron flux at the detector. In this case, a longer exposure time is needed to achieve the same level of measurement confidence because of the lower neutron count rate as discussed in the measurement uncertainty section. The neutron flux measured at the detector for the aperture setting reported here is $\Phi_0 \approx 2 \times 10^6$ (cm^{-2} s^{-1}).[9]

Detector.— Prior attempts to investigate lithium ion batteries using neutron imaging[5] were limited by the resolution of the imaging system. The thickness of commercial electrode materials[1,4] require very high resolution detectors. The cross-strip anode Micro-Channel Plate (MCP) detector used in this work is capable of resolving features on the order of 13.5 μm. This high resolution detector enables the measurement of lithium concentration across the solid phase of commercial battery electrodes, as the typical electrode thickness is between 40 and 100 μm.

Neutron capture, in a thin layer of the detector, causes the release of electrons into the MCP pores. The electric signal is then amplified, and spatially resolved using an array of wires.[17] Neutron capture events in the detector can be localized to an area 5×5 μm, which is the pixel size of the image acquired by the electronics. Hence, the best achievable detector resolution based on the sensor array is slightly larger than twice the pixel size. In practice the dimensions of the MCP pores limit the overall detector resolution.[18] The detector resolution was characterized based on independent measurement.[9] The point spread function (PSF) of this detector resolution can be modeled by a Gaussian kernel with $\sigma_D = 9.2$ μm. The corresponding FWHM of the detector is $FWHM_D = 2.35\ \sigma_D = 21.6$ μm.

Pouch cell.— As was discussed before, the pouch cell used for this experiment consists of alternating double-sided current collectors; $LiFePO_4$ on aluminum for the positive electrode and carbon on copper for the negative electrode, as shown in Fig. 5 and in the lower schematic of Fig. 6. The electrodes are separated by a porous membrane separator material to create the battery cell. The negative electrode thickness is ≈37 μm (each side) graphite with 10 μm copper foil backing. The positive electrode is 53 μm (each side) with 20 μm aluminum foil backing. The separators are 25 μm thick. The multi-layer sheets of electrode material are then folded to produce a ten layer pouch cell. The battery fixture was aligned using a stepper motor so that the optical axis was parallel to the electrode sheets. The width of the pouch cell, along the optical axis, is $\delta = 2$ cm. The capacity of the pouch cell is approximately 120 mAh.

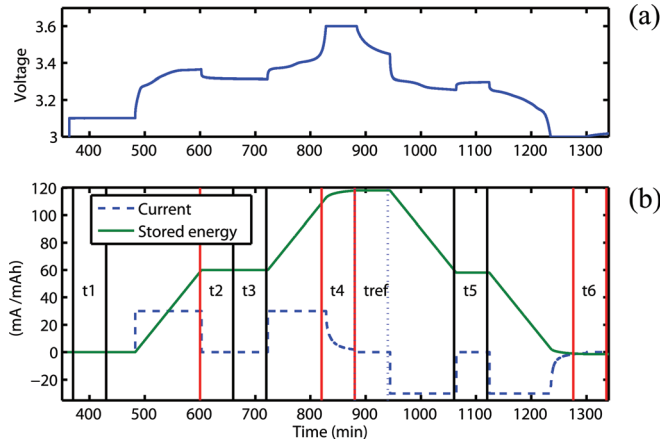

Figure 4. (Color online) Charge and discharge profile applied to the battery during imaging.

Experimental procedure.— The experiments were performed using low C-rates and long rest times to allow long exposure time in order to reduce the uncertainty in the measured lithium

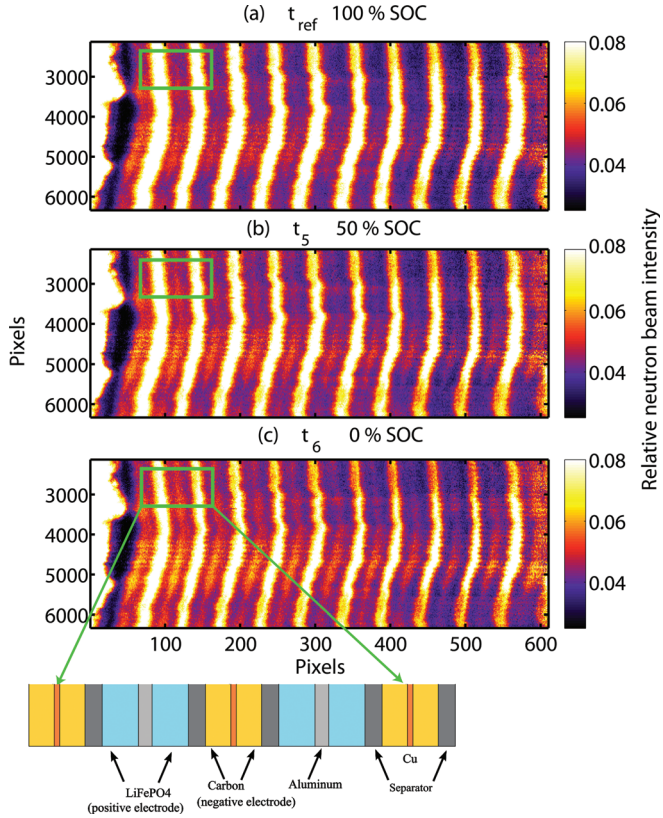

Figure 5. (Color online) Images from the charge and discharge profile corresponding to time t^{ref}, t_5, and t_6. Neutron intensity values in the images are relative (I/I_0) to the open beam intensity.

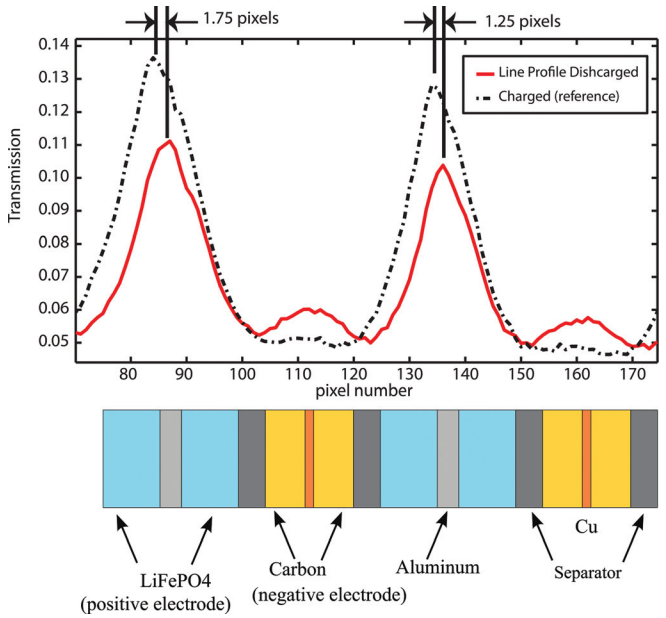

Figure 6. (Color online) The two left most peaks from the line profile of neutron transmission through the battery, from the green squares in Fig. 5, are shown with a schematic of the pouch cell showing only two folds. The total thickness of each unit battery is 260 μm, which agrees well with the average peak spacing of 52.5 pixels or 262.5 μm. Expansion of the active material during charging is visible in the peak shift. This figure shows the left-most peak which is furthest from the mounting plate and therefore subject to the greatest translational motion.

concentration. Images are acquired continuously during the experiment with a 2 min exposure time for each. Fig. 4b shows the current profile applied to the battery (dashed line) and the stored charge in mAh (solid line). The resulting voltage profile is shown Fig. 4a. The initial state of the battery was discharged, and let to rest overnight at 3.1 V. The battery is charged at C/5 rate (where C is the battery capacity) for 2.5 h to 50% state of charge (SOC) and then left to rest for 2 h, corresponding to the intervals t_2 and t_3. The battery was then charged to 100% SOC using a constant-current, constant-voltage (3.6 V) charging algorithm (t_4). The battery is then left to rest for 1 h (t_{ref}). This relaxed state at fully charged conditions, where most of the mobile lithium ions are expected to be intercalated into the carbon or negative electrode, corresponds to the reference state against which other images are compared.

The battery was then discharged to 50% SOC at C/5 rate and left to rest for 1 h, at time t_5 indicated in Fig. 4. The discharge continued to 3 V, or 0% SOC, and a final interval is defined for the rest conditions (t_6).

Observations

Images with 60 min effective exposure time, acquired during the rest periods, are calculated from the average of the 2 min exposures taken during each interval and shown in Fig. 5. These images are compressed versions of the raw image shown in Fig. 3 that are formed by averaging every 25 pixels in the y-direction. The spatial averaging is used to reduce noise increasing the signal to noise ratio and making the battery features visible in the image. The bright spots in the image correspond to the aluminum current collector, as shown in the diagram of the electrode layers at the last panel of Fig. 5. In addition to the electrode curvature along the y-axis, which is clearly visible and can be corrected by post processing, the curvature and roughness of the surface along the beam path contributes to the lower spatial resolution and cannot be corrected by post processing the images. Therefore in future experiments more care will be taken to ensure the flatness of the battery layers.

Despite the blurred electrode structure, distinct changes during charging can be observed. Specifically, Fig. 5 shows three steady state images of the relative neutron transmission through the pouch cell at t_{ref} (100% SOC), t_5 (50% SOC) , and t_6 (0% SOC). The reference state is taken to be fully charged, so that lithium accumulation (a decrease in neutron transmission) occurs in the cathode layer when the battery is discharged relative to the reference. The negative electrode (carbon) is losing lithium, therefore, the transmission increases from t_4 to t_6 in these regions. The bright region near the center of the carbon electrode develops during discharging of the battery as this region is delithiated. Supplementary material including movies of the neutron images showing the lithium migration can be found in Ref. 22.

Line profile data.— A reduction of the measurement uncertainty, due to the random nature of the neutron arrivals, can be achieved by increasing the exposure time of the image and counting more neutrons, but then the decreased temporal resolution may be unsuitable for imaging transient behavior such as battery charging.

Another approach to reducing the measurement variance is to average many pixels together over a region with uniform characteristics, in this case the lithium concentration along the electrode. By treating each pixel as an independent measurement and taking a spatial average we can achieve the same effect as increasing the exposure time by trading off in-plane resolution. A planar, one-dimensional (1D), battery structure allows for the calculation of line-profiles, where pixels along the y-axis of the image are averaged to create a 1D sectional view (across the x-direction) of the battery with much higher measurement confidence. Since the intent is to measure the change in lithium concentration across the electrode (in the x-direction or through plane), and the concentration along the electrode (along the y-axis or in-plane) should be uniform, averaging along the in-plane direction is an acceptable compromise. Therefore line-profiles, where approximately 1000 pixels along the y-direction are averaged together, are used for further data analysis and discussion. The line profile shown in Fig. 6, is calculated based on 1000 pixel average from the image shown in Fig. 5, as indicated by the rectangular box. The peaks in the line profiles are caused by the aluminum foil current collector which has an order of magnitude lower neutron attenuation than other materials in the pouch cell. The total thickness of each unit battery is 260 μm, which agrees well with the average peak spacing of 52.5 pixels or 262.5 μm. The highest attenuation is expected to come from the separator region, since it consists of plastic material that strongly attenuates neutrons. But the separator is not easy to identify in either the images or line-profile, due to its thinness ($\approx$25μm) and its proximity to the active material. The line profile clearly shows the change in lithium from anode to cathode when comparing the charged and discharged states. The charged state (dotted line) has most of the lithium in the anode and exhibits lower neutron transmission in the anode as compared to the discharged state (solid line).

Expansion of electrode materials (swelling during charge).— The pouch cell is secured to an aluminum fixture on the right side of the image near pixel 600, and therefore material expansion will produce a shift with increasing displacement (from right to left or decreasing pixel number) as the layers each expand. The peaks in the line profile, which correspond to the aluminum current collector for the positive electrode, provide the most well defined feature for determining the amount of translational motion occurring during charging. Due to the noise present in the image and in the line profile, estimation of the peak height and location is necessary, rather than simply finding the maximum value. The estimated of the peak location is found by fitting a Gaussian kernel

$$f(x) = a\exp\left(\frac{(x-\bar{x})^2}{2\sigma^2}\right) + b \qquad [2]$$

locally to the data using least-squares algorithm with four parameters (σ, $\bar{x}$, a, b) to determine the peak location, $\bar{x}$, with sub-pixel resolution.

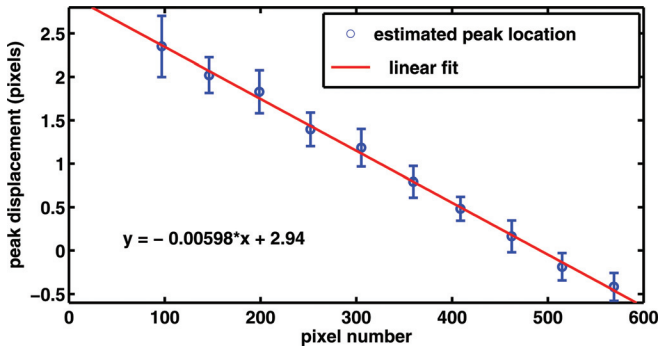

Figure 7. (Color online) Peak displacements for each of the ten layers, from the fully charged reference state to the discharged state. Positive displacement indicates a shift in the peak location to the right during discharge. Each pixel corresponds to 5 μm. The error bars indicate 95% confidence bounds in the fit of peak location parameter $\bar{x}$.

The measured peak displacements are shown in Fig. 7, and indeed, follow the linearly increasing shift pattern with the distance away from the fixed mount. The average peak displacement over the ten layers is 1.6 μm per electrode sandwich layer. This change in length corresponds to 0.6% of the total battery thickness (260 μm), or a 2% change if attributed solely to the anode active material (74 μm), which is within the range of 0–7% predicted by Fuller, et al.[19] Shrinkage of the active material is observed upon discharging consistent with the assumption of expansion due to Li intercalation.

Corrected Line Profiles and Optical Density.— Expansion of anode solid electrode material during lithium intercalation,[19] requires special attention to correctly interpret the neutron radiographs. The change in lithium concentration at time t as compared to a reference time, t_{ref} , is proportional to the optical density Eq. 3,[9] assuming no other material changes and nothing else within the image is moving. The negative logarithm of the ratio of two measurements of the beam intensity is referred to as the optical density (OD)

$$OD^{t_{ref}}(t) = -\ln\left(I(t)/I(t_{ref})\right) \propto \left(C_{Li}(t) - C_{Li}(t_{ref})\right) \qquad [3]$$

Movement of the active material, as suggested by the peak misalignment shown in Fig. 6, may lead to an erroneous estimate of the change in lithium concentration. Therefore, there is a need to estimate and correct for the expansion/contraction of the pouch cell for calculation of the optical density during charging and discharging.

The reference line profile is stretched, using an affine transformation (linear interpolation) to match the peak locations. This linear scaling of the reference transmission line profile is necessary for calculating the optical density using Eq. 3, and shown in Fig. 8b, so that the same regions of the active material are compared and valid results can be obtained. Despite the non-uniformity in the detected transmission line profile shown in Fig. 8a, the optical density shows fairly uniform change in Li concentration between pouch layers. A zoomed plot showing the change in optical density for the first two layers is shown in Fig. 9. The optical density is proportional to the change in lithium concentration; thus the only expected non-zero values of optical density should occur in the regions corresponding to the anode and cathode active material. The reference state is taken to be fully charged, so that lithium accumulation (positive values of optical density) occurs in the cathode layer when the battery is discharged relative to the reference. The negative electrode is losing lithium, therefore, the optical density decreases. The decrease in optical density in the anode and analogous increase in the cathode during discharge is shown at 50 and 0% SOC in Fig. 9.

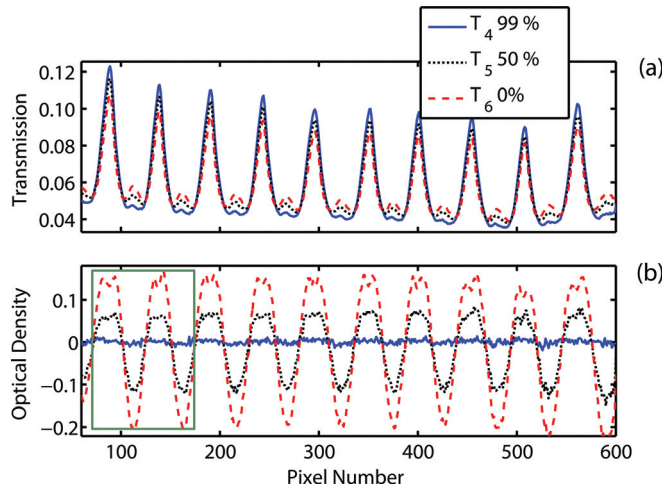

Figure 8. (Color online) Line profile of the neutron transmission at various states of charge. There is clearly variability of the neutron transmission through each fold. The optical density in the second subplot relates directly to the change in lithium concentration in the solid. Hence the mobility of Li in each fold seems to be uniform across all folds despite the observed difference in the transmission. The reference state is taken to be fully charged, so that lithium accumulation (positive values) occurs in the cathode layer when the battery is discharged relative to the reference.

Uncertainty Analysis

The neutron images are discrete measurements of the number of neutrons captured by the detector over an area $A = \Delta_y \Delta_x$ and time $\Delta_T = 120$ s, denoted by $I[i, j, k]$. Where i and j represent the spatial coordinates of the pixel, and k represents the time that the image frame was captured. The number of detected neutrons, over an area A and time T , can be described by a Poisson distributed random variable. The measurement uncertainty in Li concentration is primarily due to the neutron counting statistics.

The change in lithium concentration can be calculated from a reference image using Eq. 3. Since σ_{Li}, is not yet calibrated for the NIST beam, as previously done for liquid water,[9] only the standard deviation in optical density can be compared with the numerical results. The optical density, however, is proportional to the change in lithium concentration so the percent measurement accuracy for optical density is the same as for the concentration measurement.

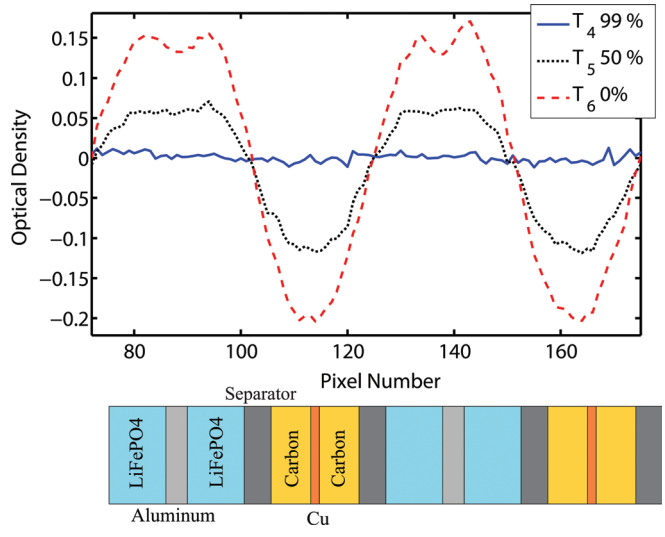

Figure 9. (Color online) Detail from Fig. 8 showing the optical density, calculated from a 4185 pixels averaged line profile of an image with a 60 min exposure, corresponding to the first two battery folds.

The theoretical standard deviation in optical density for the image data is given by the following equation

$$STD(OD^{t_{ref}}[k]) = \sqrt{\frac{1}{\lambda} + \frac{1}{\lambda^{ref}}} \quad [4]$$

where λ and λ^{ref} are the expected number of neutrons per pixel counted in the image of interest the reference image respectively. This equation indicates that the measurement uncertainty can be reduced by counting more neutrons. For a Poisson random variable, the parameter λ represents both the mean and variance of the number of counted neutrons, hence, the variance can be predicted by estimating the mean using Eq. 6. The expected number of neutrons counted by the detector for a single pixel is related to the average neutron flux at the detector surface I(x,y,t) given by Eq. 1

$$E[I[i,j,k]] = \eta \int_{\Delta_y} \int_{\Delta_x} \int_{\Delta_T} I(x,y,t)dx\,dydt = \lambda \quad [5]$$

where $\eta = 0.2$ is the detector efficiency.

When using the high resolution detector the area corresponding to a single pixel is very small since $\Delta_y = \Delta_x = 5 \times 10^{-4}$ cm are the pixel dimensions. Although the incident flux ϕ_0 is very high, on average only 10.84 neutrons per pixel per image (120 s) are detected with an open beam (no sample placed in front of the detector). The number of counted neutrons is further reduced by attenuation through the battery where placed in front of the detector. For the experimental setup described in this work, the average transmission through the battery was

$$\hat{\lambda} = \frac{1}{N_x N_y} \sum_{i=1}^{N_x} \sum_{j=1}^{N_y} I[i,j,1] = 0.64 \quad [6]$$

detected neutrons per pixel in a frame (120 s). Due to the low neutron counting rate there is a high probability that for any given pixel in the image, no neutrons will be detected over the 2 min exposure. In this case calculation of the optical density using Eq. 3, on a per-pixel basis, will result in some pixels with undefined values.

In order to overcome the statistical uncertainty (and the systematic bias of a Poisson distribution with low mean) a sufficient number of neutrons need to be counted, i.e. λ should be large. Therefore, line profiles are calculated from the image data, where pixels from regions of the battery with the same lithium concentration are averaged both in time and space (across multiple images). The pixels corresponding to the same lithium concentration (and same background attenuation) can be taken as independent measurements and used to reduce the uncertainty. The line profile corresponding to summing N_{pix} pixels along the y-axis and a 60 min effective exposure time ($N_{\text{frames}} = 30$) is given by

$$L_{P,60}[i,k] = \sum_{j=1}^{N_{pix}} \sum_{m=1}^{N_{frames}} I[i,j,k+m] \quad [7]$$

The sum of independent Poisson random variables is also Poisson distributed. Therefore, the line profile data is also described by a Poisson distribution, with parameter λ_N equal to the sum of that for each pixel. Therefore, the mean and variance of the line profile data are both equal to λ_N, and given by the following expression

$$\lambda_N = N_{pix} N_{frames} \lambda \quad [8]$$

The theoretical standard deviation in optical density for the line profile data is given by the following equation

$$STD\left(OD_{LP}^{t_{ref}}[k]\right) = \sqrt{\frac{1}{N_{frames}N_{pix}}} \sqrt{\frac{1}{\lambda} + \frac{1}{\lambda^{ref}}} \approx \sqrt{\frac{1}{N_{frames}N_{pix}}} 1.76 \quad [9]$$

An estimate of the measurement uncertainty can be found using the measured variance in number of counted neutrons neutron $\hat{\lambda}$, where $\lambda \approx \lambda^{ref} \approx \hat{\lambda} = 0.64$ neutrons per pixel. Therefore, for a 60 min exposure (30 frames) we need 4000 pixels to get STD(OD) = 0.005, or about 2.5% of the optical density corresponding to the change in lithium concentration between charged and discharged states of the battery. This theoretical value for standard deviation in optical density agrees quite well with the measured standard deviation of the 4000 pixel line profile data shown in Fig. 9.

Modeling the Image Formation and Capture Process

The image formation process introduces several artifacts changing the ideal line profile from that shown in Fig. 10a into the smoother line profile shown by Fig. 10b. This smoothing process complicates the quantification of the lithium concentration from the detected signal. So a model of the imaging process and the blurring artifacts was derived to compare with the experimental results. These artifacts are caused by at least four things; improper alignment of the battery with respect to the neutron beam, geometric unsharpness due to the pinhole imaging system, roughness or curvature of the object (non-parallel layers), and blurring of the signal introduced by the detector. Proper alignment of the battery layers, parallel to the optical axis, is critical to produce the expected transmission line profile. If the battery is slightly misaligned (rotation about the y-axis), if the layers have very rough surfaces, or if the electrodes are not flat, the transmission line profile corresponding to the various layers in the battery may appear blurred due to neutron transmission through two or more layers of the pouch cell.

Figure 10 shows a schematic of a lithium-ion pouch cell and corresponding simulation of the resulting ideal transmission line profile

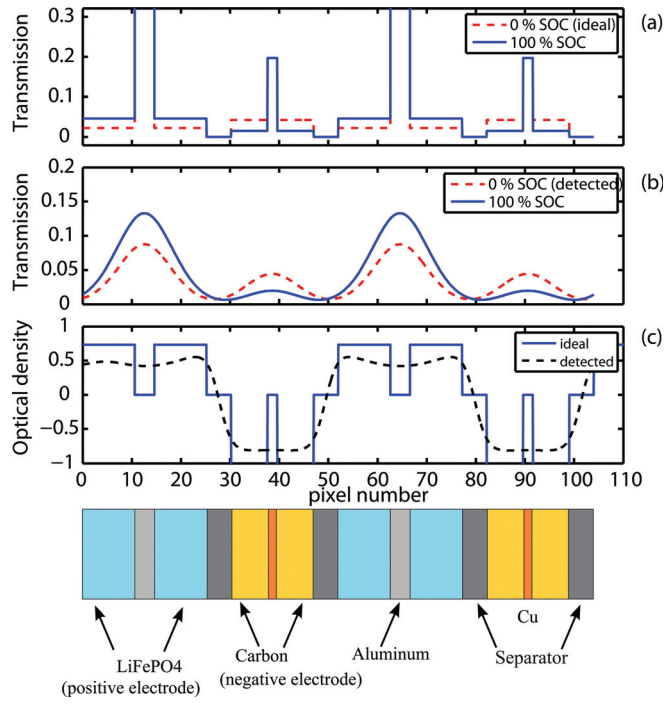

Figure 10. (Color online) A model of the transmission line profiles based on the layer structure of the Li-ion pouch cell (bottom) is shown. Dashed lines correspond to discharged state 0% SOC, and solid lines to 100% SOC. The ideal model of neutron transmission line profile is shown in subplot (a). The detected transmission line profile is shown in subplot (b), after a 0.09° rotation of the pouch cell with respect to the beam, and accounting for the blurring associated with neutron capture process in the detector. Ideal simulated optical density (solid line) and optical density resulting from the blurred transmission line profiles (dashed line) with the reference taken at the fully charged state are shown in subplot (c).

according to the Lambert-Beer law Eq. 1. The ideal line profile, shown in subplot (a), corresponding to the fully charged state is drawn with a solid line. The discharged state is shown with a dashed line. Using modeling results from Comsol, which are based on the work by Fuller, Doyle, and Newman,[1,19,20] a uniform Li concentration across the electrode is expected due to the low C-rate. Some typical material parameters are taken from the literature and applied in the model of the image formation process. Details about the model and the parameters will be documented in a future publication.

The ideal line profile is convolved with four point spread functions (PSF)s, to simulate the blurring.[9] The geometric unsharpness is captured by convolution with a rectangular function of width U_g. The rotation about the *y*-axis can be modeled by convolution with a rectangular function of width $U_r = \delta\ sin(\theta)$, where θ is the rotation and δ is the battery width. The waviness or curvature of the electrode along the optical axis can also be described by convolution with a Gaussian PSF, however the σ_w associated with this effect is unknown. Finally, the detector effect is modeled by a Gaussian PSF, with parameter σ_d. The simulated line profile, which accounts for the image degradation, is shown in Fig. 10. The simulated transmission line profile in (b) can be compared with the actual (measured) line profile in Fig. 6.

It is important to note that the overall system resolution could be much less than the detector resolution as a result of these compounded effects. This model of the blurring process is needed to extract quantitative data for the local change in lithium concentration from the optical density, which is calculated from the measured (blurry) data. Direct calculation of the optical density (change in Li concentration) using the blurred transmission line profile (dashed line) yields a lower value than the ideal (solid line), as shown in Fig. 10c. Deconvolution of the data, to reconstruct the ideal line profile is not possible as this would intensify the noise present in the signal.[21] Therefore, the ideal transmission line profile is filtered in order to compare the measured data with the expected results. Figure 10 shows good agreement with the blurred peaks in the transmission line profile, in particular the peak near pixel #38, corresponding to the anode active material in the discharged state, which becomes flat during charged conditions. Quantitative assessments of the change in lithium concentration distribution across the electrode requires calibration of the measurement tool using a lithium fluoride standard by NIST neutron imaging facility, which is currently in progress and once completed will allow the translation of measured optical density into the change of lithium concentration in the solid electrode.

Conclusion

Measurement of the change in lithium concentration between neutron radiographic images can be calculated from the optical density using the Beer-Lambert law. The experimental results with a LFP pouch cell show reasonable matching with the numerical simulation for the optical density obtained from a model of the lithium distribution in the solid electrodes during cycling of the battery at low C-rate. Spatial averaging (line profiles) and temporal averaging are utilized to overcome the statistical variance of the Poisson distribution neutron count (pixel intensity in the image). This time-averaging necessitated using low C-rate for the data reported here. The local change in neutron transmission due to the movement of lithium is clearly visible in the image data obtained by a high-resolution detector. The repeated pattern of folds inside the pouch cell provides additional confidence in interpreting the observed phenomena such as electrode swelling during charging since the dimensional change of each fold is less than the pixel size. The swelling can be attributed to a 2% change in the thickness of the anode electrode due to the lithium intercalation inside the carbon structure.

The artifacts introduced by the imaging system need to be considered when making quantitative assessments of the change in lithium concentration. Ideally, the optical density is proportional to lithium concentration. In practice, however, attempts to calculate the change in lithium concentration directly from the line profile data underestimate the change in Li concentration due to the small feature size (electrode thickness) relative to the overall resolution of the optical system. Convolving a model of an ideal line profile with a model of the image system is necessary to compare with the experimental results.

Future work will aim to measure the spatiotemporal distribution of lithium across the two electrodes during charging and discharging at various C-rates. The concentration measurements can then be used to validate models for battery management in applications that require high power demand and hence need accurate estimates of the bulk electrode-distributed Li concentration. The measurements fill a critical gap in the experimental verification and availability of *in situ* lithium concentration distributions for Li-ion batteries.

Acknowledgment

The authors thank Dr. Ding from TARDEC; Patrick Hagan, Maha Hammoud, and Danny King from A123 systems; Eli Baltic from the NIST Physical Measurement Laboratory; and Levi Thompson, Xiaohui Chen, Binay Prasad, Sun Bo Hwang, and Saemin Choi from the University of Michigan. We acknowledge the support of the National Institute of Standards and Technology, U.S. Department of Commerce, in providing the neutron research facilities used in this work. This work has been partially supported by the Ford Motor Company (Ford/UMICH Alliance Project) and by the Automotive Research Center (ARC) a U.S. Army center of excellence in modeling and simulation of ground vehicles.

University of Michigan assisted in meeting the publication costs of this article.

References

1. M. Doyle, T. F. Fuller, and J. Newman, *J. Electrochem. Soc.*, **140**, 1526 (1993).
2. K. Smith, *IEEE Control Syst. Mag.*, **30**, 18 (2010).
3. S. Santhanagopalan, Q. Zhang, K. Kumaresan, and R. E. White, *J. Electrochem. Soc.*, **155**, A345 (2008).
4. K. Smith, C. Rahn, and C.-Y. Wang, *IEEE Trans. Control Syst. Technol.*, **18**, 654 (2010).
5. M. Kamata, T. Esaka, S. Fujine, K. Yoneda, and K. Kanda, *J. Power Sources*, **68**, 459 (1997), Proceedings of the Eighth International Meeting on Lithium Batteries.
6. M. Lanz, E. Lehmann, R. Imhof, I. Exnar, and P. Novák, *J. Power Sources*, **101**, 177 (2001).
7. S. J. Harris, A. Timmons, D. R. Baker, and C. Monroe, *Chem. Phys. Lett.*, **485**, 265 (2010).
8. M. A. Rodriguez, M. H. V. Benthem, D. Ingersoll, S. C. Vogel, and H. M. Reiche, *Powder Diffr.*, **25**, 143 (2010).
9. D. S. Hussey, D. L. Jacobson, M. Arif, K. J. Coakley, and D. F. Vecchia, *J. Fuel Cell Sci. Technol.*,**7**, 021024 (2010).
10. http://www.ncnr.nist.gov/resources/n-lengths/list.html for NIST, Neutron Scattering Lengths and cross sections. Last accessed Dec 6, 2010.
11. E. Lehmann, P. Boillat, G. Scherrer, and G. Frei, *Nucl. Instrum. Methods Phys. Res. A*, **605**, 123 (2009).
12. M. A. Hickner, N. P. Siegel, K. S. Chen, D. S. Hussey, D. L. Jacobson, and M. Arif, *J. Electrochem. Soc.*, **155**, B294 (2008).
13. J. B. Siegel, D. A. McKay, A. G. Stefanopoulou, D. S. Hussey, and D. L. Jacobson, *J. Electrochem. Soc.*, **155**, B1168 (2008).
14. W. Tiedemann and J. Newman, *J. Electrochem. Soc.*, **122**, 1482 (1975).
15. D. D. Domenico, A. G. Stefanopoulou, and G. Fiengo, *ASME J. Dyn. Syst., Meas., Control*, In press.
16. A. A. Harms, and D. R. Wyman, *Mathematics and Physics of Neutron Radiography*, Springer, New York (1986).
17. A. Tremsin, O. Siegmund, and J. Vallerga, *IEEE Trans. Nucl. Sci.*, **52**, 1755 (2005).
18. O. Siegmund, J. Vallerga, A. Tremsin, and W. Feller, *IEEE Trans. Nucl. Sci.*, **56**, 1203 (2009).
19. T. F. Fuller, M. Doyle, and J. Newman, *J. Electrochem. Soc.*, **141**, 982 (1994).
20. M. Doyle, T. F. Fuller, and J. Newman, *Electrochim. Acta*, **39**, 2073 (1994).
21. F.-X. Dupe, M. Fadili, and J. Starch, in *International Conference on Acoustics, Speech and Signal Processing*, IEEE, p. 761 (2008).
22. http://www.youtube.com/user/umichfccl, Neutron Imaging of Lithium Concentration in LFP Pouch Cell Battery, Last accessed March 1, 2011.